



Controllable Synthesis of 2D Nonlayered Cr₂S₃ Nanosheets and Their Electrocatalytic Activity Toward Oxygen Evolution Reaction

Tofik Ahmed Shifa^{1,2*}, Raffaello Mazzaro³, Vittorio Morandi³ and Alberto Vomiero^{1,2*}

¹Division of Materials Science, Department of Engineering Sciences and Mathematics, Luleå University of Technology, Luleå, Sweden, ²Department of Molecular Sciences and Nanosystems, Ca' Foscari University of Venice, Venezia, Italy, ³CNR-IMM Bologna Section, Bologna, Italy

OPEN ACCESS

Edited by:

Hassan M. A. Hassan,
Suez University, Egypt

Reviewed by:

Dongpeng Yan,
Beijing Normal University, China
Guangbo Chen,
Technische Universität Dresden,
Germany

*Correspondence:

Tofik Ahmed Shifa
tofik.ahmed.shifa@ltu.se
Alberto Vomiero
alberto.vomiero@ltu.se

Specialty section:

This article was submitted to
Catalytic Engineering,
a section of the journal
Frontiers in Chemical Engineering

Received: 30 April 2021

Accepted: 07 June 2021

Published: 25 June 2021

Citation:

Shifa TA, Mazzaro R, Morandi V and Vomiero A (2021) Controllable Synthesis of 2D Nonlayered Cr₂S₃ Nanosheets and Their Electrocatalytic Activity Toward Oxygen Evolution Reaction. *Front. Chem. Eng.* 3:703812. doi: 10.3389/fceng.2021.703812

The design of oxygen evolution reaction (OER) electrocatalysts based on Earth-abundant materials holds great promise for realizing practically viable water-splitting systems. In this regard, two-dimensional (2D) nonlayered materials have received considerable attention in recent years owing to their intrinsic dangling bonds which give rise to the exposure of unsaturated active sites. In this work, we solved the synthesis challenge in the development of a 2D nonlayered Cr₂S₃ catalyst for OER application *via* introducing a controllable chemical vapor deposition scheme. The as-obtained catalyst exhibits a very good OER activity requiring overpotentials of only 230 mV and 300 mV to deliver current densities of 10 mA cm⁻² and 30 mA cm⁻², respectively, with robust stability. This study provides a general approach to optimize the controllable growth of 2D nonlayered material and opens up a fertile ground for studying the various strategies to enhance the water splitting reactions.

Keywords: 2D materials, nonlayered materials, metal sulfides, chemical vapor deposition, oxygen evolution reaction

INTRODUCTION

Designing efficient water splitting catalysts is central to substantial progress for the sustainable development of modern society (Gray, 2009; Cook et al., 2010). In this respect, the production of hydrogen through the electrolysis of water at the cathode highly depends on efficient and stable oxygen evolution reaction (OER) at the anode. However, the OER process involves proton-coupled four-electron-transfer reactions exhibiting sluggish kinetics and higher energy demands compared to the reaction at the cathode counterpart (Gao et al., 2017; Tahir et al., 2017; Yao et al., 2018; Zhang et al., 2020; Arif et al., 2021). The past few decades have witnessed rapid advances in two-dimensional (2D) materials and other materials to improve their catalytic efficiency with manifold strategies (Geim and Grigorieva, 2013; Bhimanapati et al., 2015; Shifa and Vomiero, 2019; Arif et al., 2020; Gao and Yan, 2020; Wan et al., 2020; Mushtaq et al., 2021). For instance, electronic structure engineering *via* incorporating dopants (Min Tan and Pumera, 2019; Dou et al., 2020), vacancies (Yang et al., 2019), strains (Oakes et al., 2016), and heterostructures (Deng et al., 2016; Shifa et al., 2018) has been communicated as a promising strategy to modify the binding energies of reaction intermediates. Yet, the nonlayered class of 2D materials has been barely studied in the catalysis of OER. Unlike the layered 2D materials (the in-plane atoms are connected *via* strong chemical bonding, and the stacking layers are combined *via* weak van der Waals interaction), nonlayered 2D materials are connected *via* chemical bonding in the 3D network. This in turn endows the family unsaturated

dangling bonds on the surface, thereby exhibiting a high-activity and high-energy surface (Wang et al., 2017). In addition to the dangling bonds, metal sulfides having higher conductivity as compared to oxides endow a conducive environment to accelerate the oxidation of the $-OOH$ intermediate and enhance O_2 gas generation (Peng et al., 2018; Joo et al., 2019). Moreover, chromium-based catalysts have recently won the attention of many research groups (Murray et al., 2010; Baek et al., 2012; Xu et al., 2018; Lin et al., 2019; Du et al., 2020; Park et al., 2020) due to the fact that Cr^3 cations exhibit a special electronic configuration (t^32g^0g), which facilitates electron transfer and electron capture. Despite this appealing feature, the realization of these materials is largely impeded by the fabrication challenges. Owing to the 3D strong bonding, it is difficult to controllably synthesize nonlayered 2D nanosheets through a mere exfoliation approach or conventional chemical vapor transport method. A promising approach has recently been reported on mica substrate using space confined CVD to synthesize Cr_2S_3 (Zhou et al., 2019; Cui et al., 2020; Xie et al., 2020). Yet, the OER performance of nonlayered metal sulfides remains far from satisfactory. In this work, we first synthesized Cr_2O_3 on a carbon fiber substrate (CF) and then controllably sulfurized it in a two-zone chemical vapor deposition furnace to get vertically oriented hexagonal Cr_2S_3 nanosheets. In the main CVD chamber, we employed two small tubes inserted into one another to saturate the vapors and direct their deposition at the desired target. The resulting sulfide could create a kinetically/energetically favorable environment for the adsorption/desorption of oxide moieties, thereby producing oxygen gas. Accordingly, in a typical three-electrode setup, it delivers current densities of 10 mA cm^{-2} and 30 mA cm^{-2} at overpotentials of 230 mV and 300 mV, respectively, with excellent stability for over 10 h of duration.

MATERIAL AND METHODS

Synthesis of Cr_2O_3 Precursor: The Cr_2O_3 precursor was synthesized on the CF substrate *via* the CVD method. Typically, 0.5 g of Cr_2O_3 powder was kept in the center of the CVD chamber and the CF substrate was kept ~ 7 cm away from the center. The chamber pressure was pumped down to about 0.1 Pa. Ar gas (50 standard cubic centimeters per minute (sccm)) was used to transport chromium oxide vapor species to the substrates. With this Ar-saturated environment, the temperature was raised to ~ 700 °C with a heating rate of 30 °C min^{-1} which lasts for 40 min. Then, the system was allowed to cool naturally, and the product (i.e., Cr_2O_3/CF) was taken for the next step.

Sulfurization of Cr_2O_3/CF : Two-zone CVD setup was employed to undergo the sulfurization reaction. In addition to the main CVD tube, we used two small tubes whose ends coincide with the heating centers in each zone to concentrate the vapor. Then, 0.5 g of S powder was kept in the front zone, and the Cr_2O_3/CF precursor was kept in the back zone. Before the reaction starts, the CVD tube was deaired *via* repeated (at least thrice) pumping and purging with Ar gas. Subsequently, the front and back zones

were simultaneously heated to ~ 200 °C and ~ 600 °C within 30 min under Ar gas (50 sccm), respectively, and the reaction was run for 60 min. Finally, the system was cooled down to room temperature and the sample was taken out to be used as an electrocatalyst without any further treatment.

Characterization

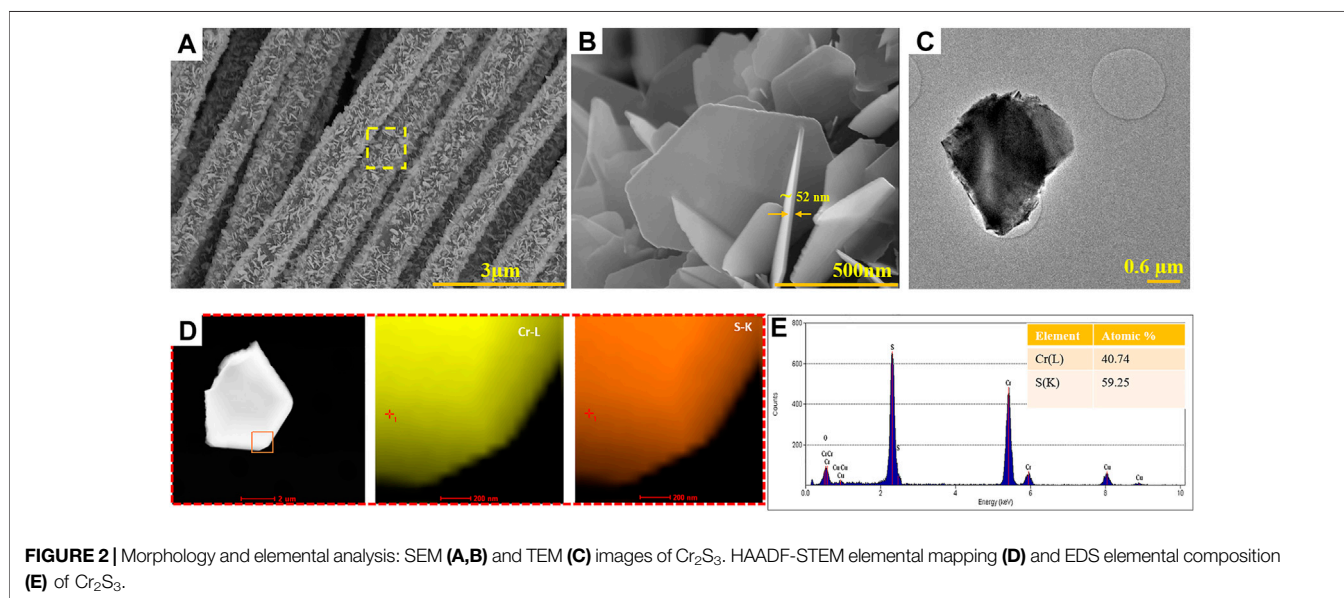
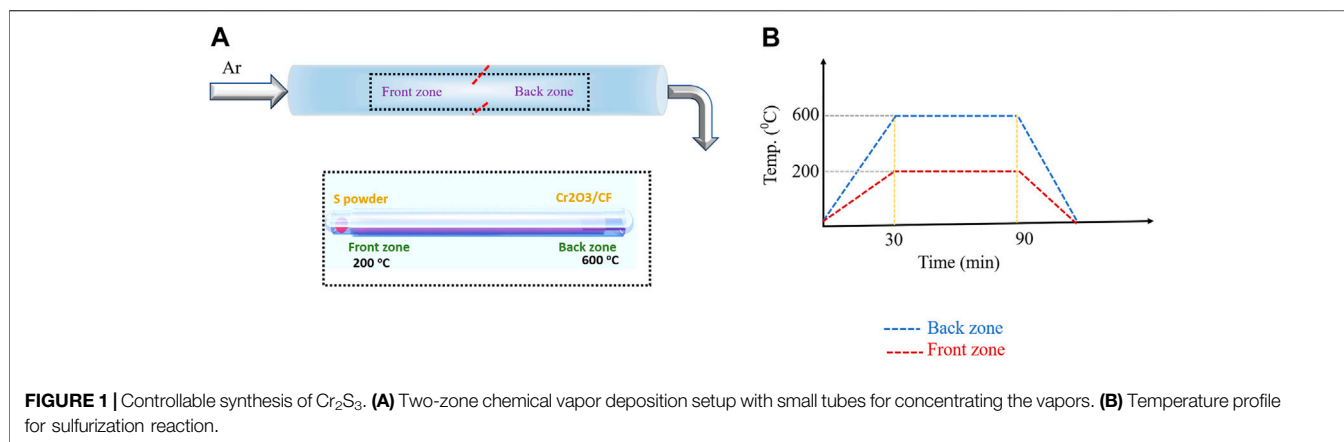
The SEM was collected *via* field emission scanning electron microscopy (FESEM), Magellan XHR 400 L, with 5 kV electron beam. The crystal structure was investigated through FEI Tecnai F20 high-resolution transmission electron microscope (HR-TEM), equipped with a Schottky emitter operating at 200 kV. Elemental analysis was performed by energy dispersive X-ray spectroscopy (EDS), equipped with scanning transmission electron microscopy (STEM-HAADF) to map elemental distribution. More crystallographic data were obtained from PanAnalytical Empyrean XRD to get the X-ray diffractogram using Cu ka radiation.

Electrochemical Measurements

ModuLab XM ECS potentiostat (Solartron Instrument) was used to measure the electrochemical properties of the as-synthesized and characterized sample. The oxygen evolution reaction catalytic performance was studied in an alkaline medium (1 M KOH) using a three-electrode configuration with an H-type electrochemical cell. Saturated calomel electrode (SCE), Pt wire, and the synthesized samples were used as the reference, counter, and working electrodes, respectively. Linear sweep voltammetry was run with a sweep rate of 5 mV/s with continuous purging of Ar gas to remove dissolved oxygen that may limit the mass transfer. All the potentials are iR corrected and presented with respect to a reversible hydrogen electrode (RHE) which was obtained from the Nernst equation: $E_{RHE} = E_{SCE} + 0.059 \text{ pH} + E_{SCE}^0$. Chronopotentiometry was run at a current density of 100 mA cm^{-2} to evaluate the stability test. Electrochemical impedance spectra (EIS) measurements were carried out from 0.1 to 100,000 Hz with an amplitude of 5 mV and overpotential of 300 mV.

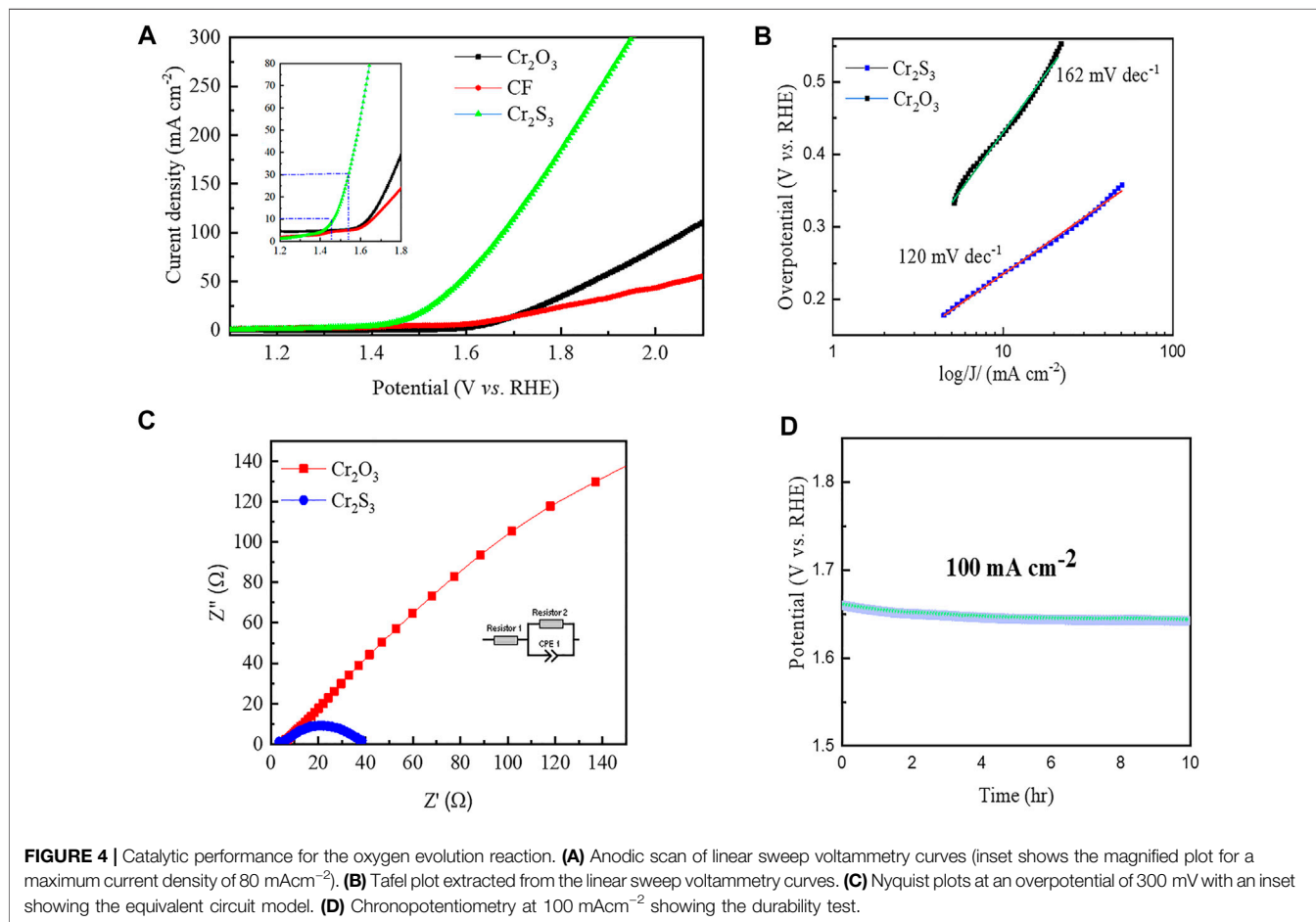
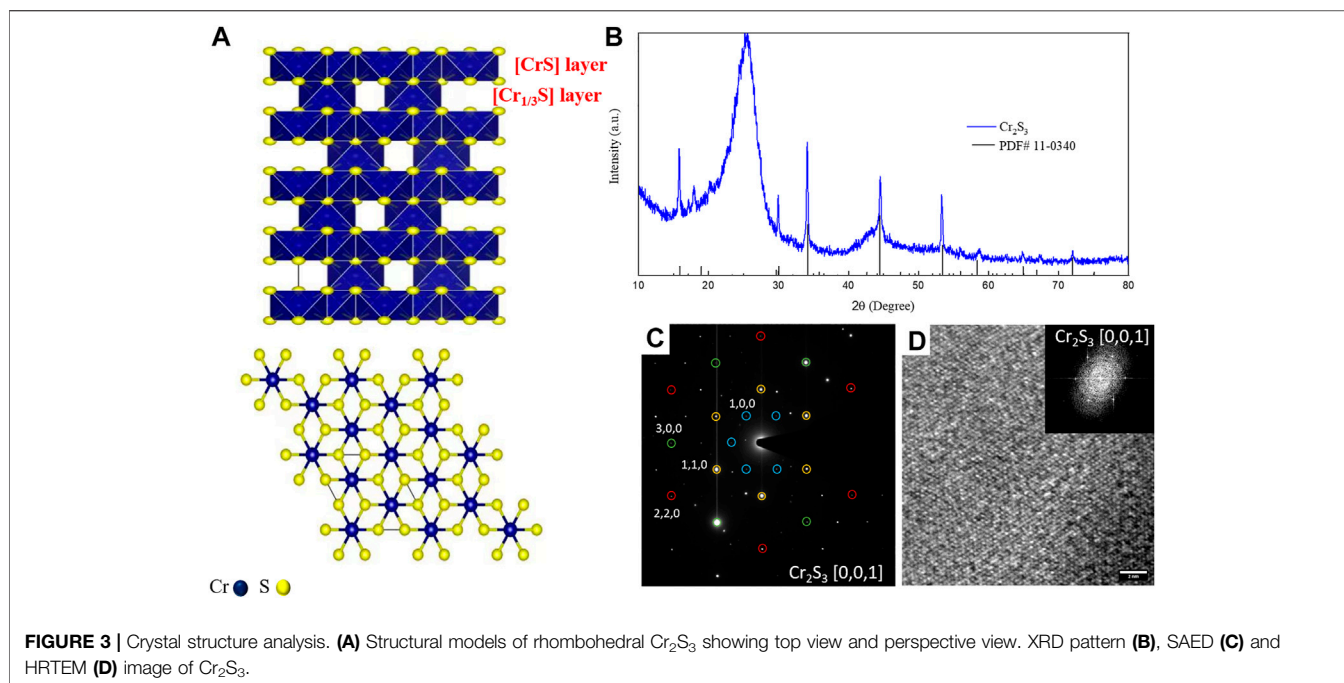
RESULTS AND DISCUSSIONS

The synthesis of Cr_2S_3 followed a two-step route. The Cr_2O_3 oxide precursor was first deposited on carbon fiber (CF) substrate *via* the chemical vapor deposition method using Cr_2O_3 powder as source. The produced material exhibits rough, platelet-like structures formed by sintered nanocrystals (**Supplementary Figure S1A**). The HRTEM micrographs and selected area electron diffraction (SAED) confirm the growth of hexagonal Cr_2O_3 on the CF substrate, as reported in **Supplementary Figures S1B–D**. The Cr_2O_3 obtained in the first step was used as a precursor for the second step which is a sulfurization process. **Figure 1** shows the employed CVD setup meant for sulfurization, wherein S powder is kept in the front zone and the Cr_2O_3/CF was kept in the back zone. The growth of Cr_2S_3 is rather challenging as it requires a confined space to control the kinetics and/or the thermodynamics of the vapor transport and thereby the



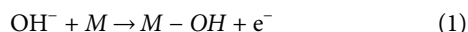
deposition process (Zhou et al., 2019). To this end, we employed two small tubes (socketed into one another as shown in **Figure 1**) to concentrate the sulfur vapor and direct to the back zone where Cr_2S_3 is formed. The temperatures in both zones are controllable and the optimized temperature profile is depicted in the left side (**Figure 1**). The morphologies of the as-obtained products were examined through field emission scanning electron microscope (FESEM) and transmission electron microscopy (TEM). As can be seen from **Figure 2A**, the marked region which is enlarged in **Figure 2B**, hexagonal-shaped nanosheets with thickness ~ 52 nm are grown entirely on the surface of the CF substrate. The TEM image also supports this observation (**Figure 2C**). The elemental composition analysis, obtained from energy dispersive spectroscopy (EDS), illustrates the presence of Cr and S with uniform distribution throughout the entire sheet and with atomic ratio affirming the desired composition (2:3). The crystal structure was analyzed *via* X-ray diffraction and high-resolution TEM (HRTEM). The perspective and top views of structural modeling are illustrated in **Figure 3A**. Typically, Cr_2S_3

exhibits a periodic stacking of CrS_6 wherein the Cr^{3+} bonded to six S^{2-} atoms forming a mixture of edge sharing (with fully occupied CrS layer) and corner/face sharing (1/3 occupied Cr1/3S layer), thereby forming a stable structure (Maignan et al., 2012). A compelling difference between nonlayered 2D Cr_2S_3 and layered 2D materials (MoS_2 and WS_2) is that the adjacent [Cr1/3S] and [CrS] layers are connected *via* strong covalent bonds rather than the weak van der Waals forces (Chhowalla et al., 2013). The XRD pattern in **Figure 3B** shows that the peaks meant for the as-synthesized Cr_2S_3 matches the standard rhombohedral Cr_2S_3 pattern (PDF #10-0,340) with distinct peaks at 2θ values of 15.7° , 17.9° , 29.9° , 34.15° , 44.59° , 53.36° , 58.7° , 64.9° , and 72.08° meant for (0,0,3), (1,0,1), (1,1,0), (1,1,3), (1,1,6), (3,0,0), (1,1,9), (2,2,3), and (2,2,6) crystal planes. The broad peak at around $2\theta = 25^\circ$ originated from the CF substrate, and there are no any other peaks associated with the oxide phase substantiating the fact that the synthesized product is indeed pure phase Cr_2S_3 (the XRD pattern of the $\text{Cr}_2\text{O}_3/\text{CF}$ precursor is provided in **Supplementary Figure S2**). To further solidify this



observation, the crystal phase was analyzed *via* HRTEM. Selected area electron diffraction (SAED) of a single platelet (**Figure 3C**) displays a sharp single crystal hexagonal pattern, indexed as rhombohedral Cr₂S₃ phase on [0,0,1] zone axis. The HRTEM displays the formation of a crystalline structure with a diffraction spot resulting from a typical pattern for Cr₂S₃ (**Figure 3D**). Moreover, there could also be some defects and/dislocations in the structure marked by the broken red lines (**Supplementary Figure S3**). It has been proved that defects favor electrocatalysis in water splitting reactions (Xie et al., 2013; Fan et al., 2018). They introduce unsaturated sites, thereby increasing the conductivity and catalytic activity.

Having proved the successful sulfurization, we tested the electrocatalytic performance toward oxygen evolution reaction (OER) *via* a three-electrode electrochemical cell consisting of saturated calomel electrode, Pt wire, and the synthesized sample (without any treatment) as reference, counter, and working electrodes, respectively. The unsulfurized (i.e., Cr₂O₃) and the bare CF samples were also tested for the sake of comparison. **Figure 4A** shows the anodic scan linear sweep voltammetry (LSV) polarization curves elucidating the electrocatalytic activity toward OER. It can be seen that the catalytic activity due to the bare substrate is negligible, substantiating the fact that the activities observed on other samples are solely from the grown materials. Accordingly, the sulfurized product exhibits a significantly improved activity toward OER as compared to the oxide counterparts. It requires overpotentials of only 230 mV and 300 mV to deliver current densities of 10 mA cm⁻² and 30 mA cm⁻², respectively. To get a clear picture of the intrinsic activity of the materials, we normalized the polarization curves with respect to electrochemically activated surface area (ECSA). **Supplementary Figure S4** illustrates that there is still a significant enhancement in the catalytic activity for Cr₂S₃ as compared to its oxide counterpart. The OER performance reported in this study is compared fairly with most of the other recently reported materials (**Supplementary Table S1**). In fact, the OER process depends on the interaction strength of various intermediates with the surface of the catalyst (**Equations 1–4**). In the case of metal oxide, the increased 3d–2P repulsion between the metal d-band center and the coordinated oxygen P-band center results in the weakening of M–OH interaction. In the case of metal sulfides, with a more electronegative S, they accelerate the formation of –OOH intermediates from the adsorbed OH, thereby generating O₂ gas (Joo et al., 2019). It is noteworthy that metal sulfides and phosphides turn into a more active surface during OER catalysis owing to the formation of the amorphous oxide phase contributing greatly to the enhancement of the catalytic reaction (Li et al., 2019; Shifa et al., 2021).



The enhanced catalytic activity after sulfurization is even more evident from the Tafel plot analysis, derived from the polarization

curve. It suggests the overpotential increment necessary to raise the current density by tenfold. **Figure 4B** shows the smaller Tafel slope for Cr₂S₃ (120 mV dec⁻¹) as compared to Cr₂O₃ (162 mV dec⁻¹). The smaller the Tafel slope, the better the kinetics of the electrochemical reaction in electrocatalysis, and hence, the OER rate will rapidly increase with the application of overpotential.

Another important figure of merits in OER catalysis is conductivity (or resistivity). Due to the low intrinsic electrical conductivity, metal oxides commonly have high charge transfer resistance, resulting in large overpotentials (Matsumoto and Sato, 1986; Liu et al., 2017). We employed electrochemical impedance spectroscopy (EIS) analysis to evaluate the charge transfer resistance (R_{ct}). As expected, the R_{ct} value (35.2Ω) of the sulfurized product is much lower than its oxide counterparts substantiated from the small semicircle in the Nyquist plot of **Figure 4C** (inset shows the equivalent circuit model, and the fitting detail is provided in the supporting information, **Supplementary Figure S5**).

Stability is a vital criterion to evaluate electrocatalysts for broader applications. The sulfurized product not only exhibits enhanced performance but also shows remarkable durability in OER catalysis. **Figure 4D** shows the chronopotentiometry result at 100 mA cm⁻², showing the long-term stability of the catalysts without noticeable degradation.

To uncover the underlying mechanism of the enhanced OER activity, we estimated electrochemical active surface area (ECSA) *via* experimentally determining the electrochemical double-layer capacitance (C_{dl}). The ECSA of a material with similar composition is proportional to its C_{dl} value, and the C_{dl} value can be obtained from the slope of a linear curve constructed from half of the change in current density vs. scan rates. For this, cyclic voltammeteries at various scan rates were run in the non-Faradaic region. The faster scan rates lead to a decrease in the size of the diffusion layer; as a consequence, higher currents are observed and thereby the current increases at faster voltage scan rates (**Figures 5A,B**). The higher value of C_{dl} for the sulfurized product in **Figure 5C** indicates that Cr₂S₃ exposes highest active sites that could be associated with the presence of unsaturated surfaces, dangling bonds, defects, and/or dislocation as has been observed in the HRTEM image (**Figure 3C**). This kind of active site exposure is supposed to be one of the possible reasons for enhanced OER performance.

CONCLUSION

In summary, we have controllably synthesized Cr₂S₃ *via* sulfurization of Cr₂O₃ in a two-zone CVD method for electrocatalysis of OER. The two small tubes inside the main CVD chamber played a critical role to confine the system and hence saturate the sulfur vapor, thereby meeting the target at the deposition zone. Various characterization techniques reveal the formation of crystalline pure phase rhombohedral Cr₂S₃ without any impurities. Benefitting from the exposed active sites, Cr₂S₃ exhibits a remarkable electrocatalytic performance toward OER in an alkaline environment. It requires only 230 mV vs. RHE to deliver a current density of 10 mA cm⁻² with robust stability for over 10 h of duration. Our synthesis design strategy is generally

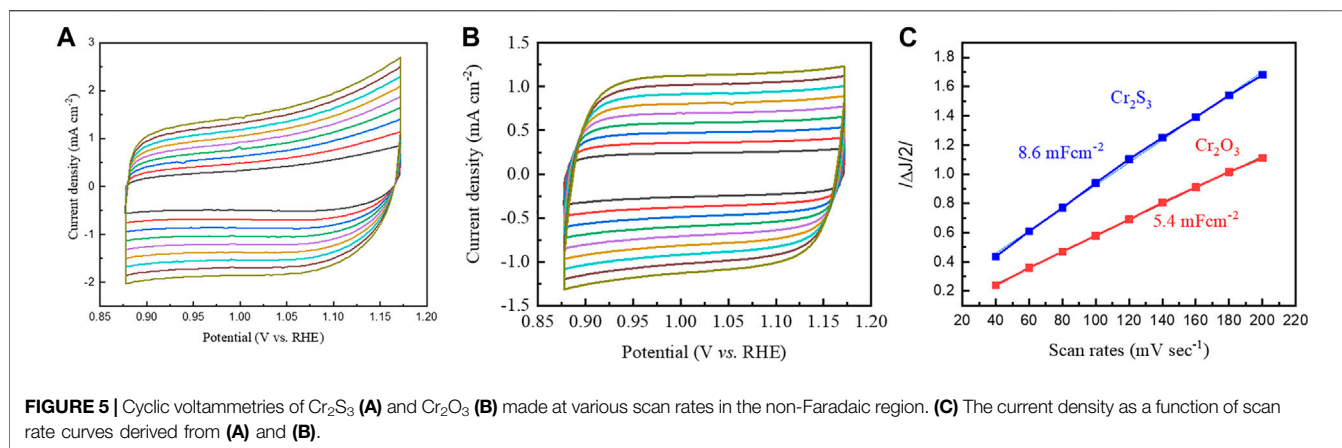


FIGURE 5 | Cyclic voltammograms of Cr₂S₃ (A) and Cr₂O₃ (B) made at various scan rates in the non-Faradaic region. (C) The current density as a function of scan rate curves derived from (A) and (B).

applicable, opening up a fresh insight into the advancement of nonlayered 2D materials. Future interest may lie in further optimization of the catalyst to be employed for overall water splitting in both acidic and alkaline media.

DATA AVAILABILITY STATEMENT

The original contributions presented in the study are included in the article/**Supplementary Material**; further inquiries can be directed to the corresponding authors.

AUTHOR CONTRIBUTIONS

TS initiated the idea, performed the synthesis, conducted characterizations, and wrote the manuscript. RM and VM conducted the TEM and interpreted the result. AV made overall supervision and led the project. All authors discussed, reviewed, and approved the manuscript.

REFERENCES

- Arif, M., Yasin, G., Luo, L., Ye, W., Mushtaq, M. A., Fang, X., et al. (2020). Hierarchical Hollow Nanotubes of NiFeV-Layered Double hydroxides@CoVP Heterostructures towards Efficient, pH-Universal Electrocatalytic Nitrogen Reduction Reaction to Ammonia. *Appl. Catal. B: Environ.* 265, 118559. doi:10.1016/j.apcatb.2019.118559
- Arif, M., Yasin, G., Shakeel, M., Mushtaq, M. A., Ye, W., Fang, X., et al. (2021). Highly Active Sites of NiVB Nanoparticles Dispersed onto Graphene Nanosheets towards Efficient and pH-Universal Overall Water Splitting. *J. Energ. Chem.* 58, 237–246. doi:10.1016/j.jechem.2020.10.014
- Baek, J., Yun, H. J., Yun, D., Choi, Y., and Yi, J. (2012). Preparation of Highly Dispersed Chromium Oxide Catalysts Supported on Mesoporous Silica for the Oxidative Dehydrogenation of Propane Using CO₂: Insight into the Nature of Catalytically Active Chromium Sites. *ACS Catal.* 2, 1893–1903. doi:10.1021/cs300198u
- Bhimanapati, G. R., Lin, Z., Meunier, V., Jung, Y., Cha, J., Das, S., et al. (2015). Recent Advances in Two-Dimensional Materials beyond Graphene. *ACS Nano* 9, 11509–11539. doi:10.1021/acsnano.5b05556

ACKNOWLEDGMENTS

The authors acknowledge the Kempe Foundation (JCK1505, JCK1703, SMK 1839), the Knut och Alice Wallenberg Foundation (grant number KAW 2016.346), the ÅFORSK Foundation, and the Luleå University of Technology for financial support. The authors would also like to thank NSC, Tetralith, for allocation of high-performance computing time and resources (projects SNIC 2019/3-450 and SNIC 2019/3-684), through the Swedish National Infrastructure for Computing (SNIC). RM and VM acknowledge the EU community (Graphene Flagship Core 3, grant agreement ID 881603).

SUPPLEMENTARY MATERIAL

The Supplementary Material for this article can be found online at: <https://www.frontiersin.org/articles/10.3389/fceng.2021.703812/full#supplementary-material>

- Chhowalla, M., Shin, H. S., Eda, G., Li, L.-J., Loh, K. P., and Zhang, H. (2013). The Chemistry of Two-Dimensional Layered Transition Metal Dichalcogenide Nanosheets. *Nat. Chem* 5, 263–275. doi:10.1038/nchem.1589
- Cook, T. R., Dogutan, D. K., Reece, S. Y., Surendranath, Y., Teets, T. S., and Nocera, D. G. (2010). Solar Energy Supply and Storage for the Legacy and Nonlegacy Worlds. *Chem. Rev.* 110, 6474–6502. doi:10.1021/cr100246c
- Cui, F., Zhao, X., Xu, J., Tang, B., Shang, Q., Shi, J., et al. (2020). Controlled Growth and Thickness-Dependent Conduction-Type Transition of 2D Ferrimagnetic Cr 2 S 3 Semiconductors. *Adv. Mater.* 32, 1905896. doi:10.1002/adma.201905896
- Deng, D., Novoselov, K., Fu, Q., Zheng, N., Tian, Z., and Bao, X. (2016). Undefined Catalysis with Two-Dimensional Materials and Their Heterostructures. *nature.com*. Available at: <https://www.nature.com/nano/journal/v11/n3/abs/nnano.2015.340.html> (Accessed June 19, 2019).
- Dou, Y., He, C.-T., Zhang, L., Yin, H., Al-Mamun, M., Ma, J., et al. (2020). Approaching the Activity Limit of CoSe₂ for Oxygen Evolution via Fe Doping and Co Vacancy. *Nat. Commun.* 11, 1664. doi:10.1038/s41467-020-15498-0
- Du, X., Su, H., and Zhang, X. (2020). Cr Doped-Co9S8 Nanoarrays as High-Efficiency Electrocatalysts for Water Splitting. *J. Alloys Compd.* 824, 153965. doi:10.1016/j.jallcom.2020.153965

- Fan, X., Liu, Y., Chen, S., Shi, J., Wang, J., Fan, A., et al. (2018). Defect-enriched Iron Fluoride-Oxide Nanoporous Thin Films Bifunctional Catalyst for Water Splitting. *Nat. Commun.* 9, 1809. doi:10.1038/s41467-018-04248-y
- Gao, R., and Yan, D. (2020). Recent Development of Ni/Fe-Based Micro/Nanostructures toward Photo/Electrochemical Water Oxidation. *Adv. Energ. Mater.* 10, 1900954. doi:10.1002/aenm.201900954
- Gao, R., Zhang, H., and Yan, D. (2017). Iron Diselenide Nanoplatelets: Stable and Efficient Water-Electrolysis Catalysts. *Nano Energy* 31, 90–95. doi:10.1016/j.nanoen.2016.11.021
- Geim, A. K., and Grigorieva, I. V. (2013). Van der Waals heterostructures. *Nature* 499, 419–425. doi:10.1038/nature12385
- Gray, H. B. (2009). Powering the Planet with Solar Fuel. *Nat. Chem* 1, 7. doi:10.1038/nchem.141
- Joo, J., Kim, T., Lee, J., Choi, S. I., and Lee, K. (2019). Morphology-Controlled Metal Sulfides and Phosphides for Electrochemical Water Splitting. *Adv. Mater.* 31, 1806682. doi:10.1002/adma.201806682
- Li, W., Xiong, D., Gao, X., and Liu, L. (2019). The Oxygen Evolution Reaction Enabled by Transition Metal Phosphide and Chalcogenide Pre-catalysts with Dynamic Changes. *Chem. Commun.* 55, 8744–8763. doi:10.1039/C9CC02845E
- Lin, Y., Tian, Z., Zhang, L., Ma, J., Jiang, Z., Deibert, B. J., et al. (2019). Chromium-ruthenium Oxide Solid Solution Electrocatalyst for Highly Efficient Oxygen Evolution Reaction in Acidic media. *Nat. Commun.* 10, 162. doi:10.1038/s41467-018-08144-3
- Liu, K., Zhang, C., Sun, Y., Zhang, G., Shen, X., Zou, F., et al. (2017). High-Performance Transition Metal Phosphide Alloy Catalyst for Oxygen Evolution Reaction. *ACS Nano* 12, 158–167. doi:10.1021/acsnano.7b04646
- Maignan, A., Bréard, Y., Guilmeau, E., and Gascoin, F. (2012). Transport, Thermoelectric, and Magnetic Properties of a Dense Cr₂S₃ Ceramic. *J. Appl. Phys.* 112, 013716. doi:10.1063/1.4736417
- Matsumoto, Y., and Sato, E. (1986). Electrocatalytic Properties of Transition Metal Oxides for Oxygen Evolution Reaction. *Mater. Chem. Phys.* 14, 397–426. doi:10.1016/0254-0584(86)90045-3
- Murray, L. J., Yano, J., Chavan, S., Bordiga, S., Brown, C. M., Long, J. R., et al. (2010). Highly-Selective and Reversible O₂ Binding in Cr₃(1,3,5-Benzenetricarboxylate)₂. *J. Am. Chem. Soc.* 132, 7856–7857. doi:10.1021/ja1027925
- Mushtaq, M. A., Arif, M., Fang, X., Yasin, G., Ye, W., Basharat, M., et al. (2021). Photoelectrochemical Reduction of N₂ to NH₃ under Ambient Conditions through Hierarchical MoSe₂@g-C₃N₄ Heterojunctions. *J. Mater. Chem. A* 9, 2742–2753. doi:10.1039/D0TA10620H
- Oakes, L., Carter, R., Hanken, T., Cohn, A. P., Share, K., Schmidt, B., et al. (2016). Interface Strain in Vertically Stacked Two-Dimensional Heterostructured Carbon-MoS₂ Nanosheets Controls Electrochemical Reactivity. *Nat. Commun.* 7, 11796. doi:10.1038/ncomms11796
- Park, H., Lee, E., Lei, M., Joo, H., Coh, S., and Fokwa, B. P. T. (2020). Canonic-Like HER Activity of Cr_{1-x}MoxB₂ Solid Solution: Overpowering Pt/C at High Current Density. *Adv. Mater.* 32, 2000855. doi:10.1002/adma.202000855
- Peng, L., Shah, S. S. A., and Wei, Z. (2018). Recent Developments in Metal Phosphide and Sulfide Electrocatalysts for Oxygen Evolution Reaction. *Chin. J. Catal.* 39, 1575–1593. doi:10.1016/S1872-2067(18)63130-4
- Shifa, T. A., and Vomiero, A. (2019). Confined Catalysis: Progress and Prospects in Energy Conversion. *Adv. Energ. Mater.* 9, 1902307. doi:10.1002/aenm.201902307
- Shifa, T. A., Wang, F., Liu, Y., and He, J. (2018). Heterostructures Based on 2D Materials: A Versatile Platform for Efficient Catalysis. *Adv. Mater.* 31, 1804828. doi:10.1002/adma.201804828
- Shifa, T. A., Yusupov, K., Solomon, G., Gradone, A., Mazzaro, R., Cattaruzza, E., et al. (2021). In Situ-Generated Oxide in Sn-Doped Nickel Phosphide Enables Ultrafast Oxygen Evolution. *ACS Catal.* 11, 4520–4529. doi:10.1021/acscatal.1c00476
- Tahir, M., Pan, L., Idrees, F., Zhang, X., Wang, L., Zou, J.-J., et al. (2017). Electrocatalytic Oxygen Evolution Reaction for Energy Conversion and Storage: A Comprehensive Review. *Nano Energy* 37, 136–157. doi:10.1016/j.nanoen.2017.05.022
- Tan, S. M., and Pumera, M. (2019). Two-Dimensional Materials on the Rocks: Positive and Negative Role of Dopants and Impurities in Electrochemistry. *ACS Nano* 13, 2681–2728. doi:10.1021/acsnano.8b07795
- Wan, W., Triana, C. A., Lan, J., Li, J., Allen, C. S., Zhao, Y., et al. (2020). Bifunctional Single Atom Electrocatalysts: Coordination-Performance Correlations and Reaction Pathways. *ACS Nano* 14, 13279–13293. doi:10.1021/acsnano.0c05088
- Wang, F., Wang, Z., Shifa, T. A., Wen, Y., Wang, F., Zhan, X., et al. (2017). Two-Dimensional Non-Layered Materials: Synthesis, Properties and Applications. *Adv. Funct. Mater.* 27, 1603254. doi:10.1002/adfm.201603254
- Xie, J., Zhang, H., Li, S., Wang, R., Sun, X., Zhou, M., et al. (2013). Defect-Rich MoS₂ Ultrathin Nanosheets with Additional Active Edge Sites for Enhanced Electrocatalytic Hydrogen Evolution. *Adv. Mater.* 25, 5807–5813. doi:10.1002/adma.201302685
- Xie, L., Wang, J., Li, J., Li, C., Zhang, Y., Zhu, B., et al. (2020). An Atomically Thin Air-Stable Narrow-Gap Semiconductor Cr₂S₃ for Broadband Photodetection with High Responsivity. *Adv. Electron. Mater.*, 2000962. doi:10.1002/aem.202000962
- Xu, D., Stevens, M. B., Rui, Y., DeLuca, G., Boettcher, S. W., Reichmanis, E., et al. (2018). The Role of Cr Doping in Ni Fe Oxide/(oxy)hydroxide Electrocatalysts for Oxygen Evolution. *Electrochimica Acta* 265, 10–18. doi:10.1016/j.electacta.2018.01.143
- Yang, J., Wang, Y., Lagos, M. J., Manichev, V., Fullon, R., Song, X., et al. (2019). Single Atomic Vacancy Catalysis. *ACS Nano* 13, 9958–9964. doi:10.1021/acsnano.9b05226
- Yao, L., Zhang, N., Wang, Y., Ni, Y., Yan, D., and Hu, C. (2018). Facile Formation of 2D Co₂P@Co₃O₄ Microsheets through *In-Situ* Topotactic Conversion and Surface Corrosion: Bifunctional Electrocatalysts towards Overall Water Splitting. *J. Power Sourc.* 374, 142–148. doi:10.1016/j.jpowsour.2017.11.028
- Zhang, B., Wang, L., Cao, Z., Kozlov, S. M., García de Arquer, F. P., Dinh, C. T., et al. (2020). High-valence Metals Improve Oxygen Evolution Reaction Performance by Modulating 3d Metal Oxidation Cycle Energetics. *Nat. Catal.* 3, 985–992. doi:10.1038/s41929-020-00525-6
- Zhou, S., Wang, R., Han, J., Wang, D., Li, H., Gan, L., et al. (2019). Ultrathin Non-van der Waals Magnetic Rhombohedral Cr₂S₃: Space-Confined Chemical Vapor Deposition Synthesis and Raman Scattering Investigation. *Adv. Funct. Mater.* 29, 1805880. doi:10.1002/adfm.201805880

Conflict of Interest: The authors declare that the research was conducted in the absence of any commercial or financial relationships that could be construed as a potential conflict of interest.

Copyright © 2021 Shifa, Mazzaro, Morandi and Vomiero. This is an open-access article distributed under the terms of the Creative Commons Attribution License (CC BY). The use, distribution or reproduction in other forums is permitted, provided the original author(s) and the copyright owner(s) are credited and that the original publication in this journal is cited, in accordance with accepted academic practice. No use, distribution or reproduction is permitted which does not comply with these terms.